15

Analog Circuits Implementing a Critical Temperature Sensor Based on Excitable Neuron Models

Gessyca M., Tovar Nunez
Hokkaido University
Japan

1. Introduction

Temperature is the most often-measured environmental quality. This might be expected since temperature control is fundamental to the operation of electronic and other systems. In the present, there are several passive and active sensors for measuring system temperatures, including thermocouples, resistive-temperature detectors (RTDs), thermistors, and silicon temperature sensors (Gopel et al., 1990) (Wang et al., 1998). Among present temperature sensors, thermistors with a positive temperature coefficient (PTC) are widely used because they exhibit a sharp increase of resistance at a specific temperature. Therefore, PTC thermistors are suitable for implementation in temperature-control systems that make decisions, like shutting down equipments above a certain threshold temperature or to turning cooling fans on and off, general purpose temperature monitors.
Here I propose a sub-threshold CMOS circuit that changes its dynamical behavior; i.e., oscillatory or stationary behaviors, around a given threshold temperature, aiming to the development of low-power and compact temperature switch on monolithic ICs. The threshold temperature can be set to a desired value by adjusting an external bias voltage. The circuit consists of two pMOS differential pairs, small capacitors, current reference circuits, and off-chip resistors with low temperature dependence. The circuit operation was fully investigated through theoretical analysis, extensive numerical simulations and circuit simulations using the Simulation Program of Integrated Circuit Emphasis (SPICE). Moreover, I experimentally demonstrate the operation of the proposed circuit using discrete MOS devices.

2. The model

The temperature sensor operation model is shown in Fig. 1. The model consists of a nonlinear neural oscillator that changes its state between oscillatory and stationary when it receives an external perturbation (temperature). The key idea is the use of excitable circuits that are strongly inspired by the operation of biological neurons. A temperature increase causes a regular and reproducible increase in the frequency of the generation of pacemaker potential in most *Aplysia* and *Helix* excitable neurons (Fletcher & Ram, 1990). Generation of the activity pattern of the Br-type neuron located in the right parietal ganglion of *Helix pomatia* is a temperature-dependent process. The Br neuron shows its characteristic bursting

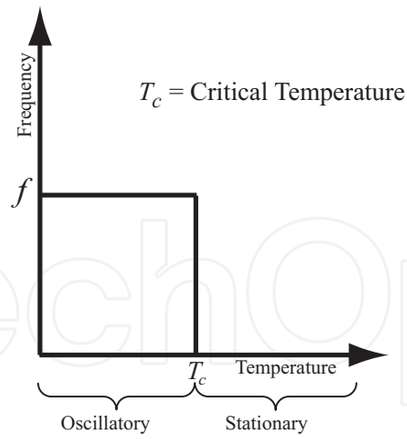

Fig. 1. Critical temperature sensor operation model.

activity only between 12 and 30°C. Outside this range, the burst pattern disappears and the action potentials become regular. This means that excitable neurons can be used as sensors to determine temperature ranges in a natural environment.

There are many models of excitable neurons, but only a few of them have been implemented on CMOS LSIs, e.g., silicon neurons that emulate cortical pyramidal neurons (Douglas et al., 1995), FitzHugh-Nagumo neurons with negative resistive circuits (Barranco et al., 1991), artificial neuron circuits based on by-products of conventional digital circuits (Ryckebusch et al., 1989) - (Meador & Cole, 1989), and ultralow-power sub-threshold neuron circuits (Asai et al., 2003). Our model is based on the Wilson-Cowan system (Wilson & Cowan, 1972) because it is easy to both analyze theoretically and implement in sub-threshold CMOS circuits.

The dynamics of the temperature sensor can be expressed as:

$$\tau \dot{u} = -u + \frac{\exp(u/A)}{\exp(u/A) + \exp(v/A)}, \tag{1}$$

$$\dot{v} = -v + \frac{\exp(u/A)}{\exp(u/A) + \exp(\theta/A)}, \tag{2}$$

where τ represents the time constant, θ is an external input, and A is a constant proportional to temperature. The second term of the r.h.s. of Eq.(1) represents the sigmoid function, a mathematical function that produces an S-shaped (sigmoid) curve. The sigmoid function can be implemented in VLSIs by using differential-pair circuits, making this model suitable for implementation in analog VLSIs.

To analyze the system operation, it is necessary to calculate its nullclines. Nullclines are curves in the phase space where the differentials $\dot{u}$ and $\dot{v}$ are equal to zero. The nullclines divide the phase space into four regions. In each region the vector field follows a specific direction. Along the curves the vector field is either completely horizontal or vertical; on the u nullcline the direction of the vector is vertical; and on the v nullcline, it is horizontal. The u and v nullclines indicating the direction of vector field in each region are shown in Fig. 2.

The trajectory of the system depends on the time constant τ, which modifies the velocity field of u. In Eq. (1), if τ is large, the value of u decreases, and for small τ, u increases. Figures 3(a) and (b) show trajectories when $\tau = 1$ and $\tau << 1$. In the case where $\tau << 1$, the trajectory on the u direction is much faster than that in the v, so only close to the u nullcline movements of vectors in vertical direction are possible.

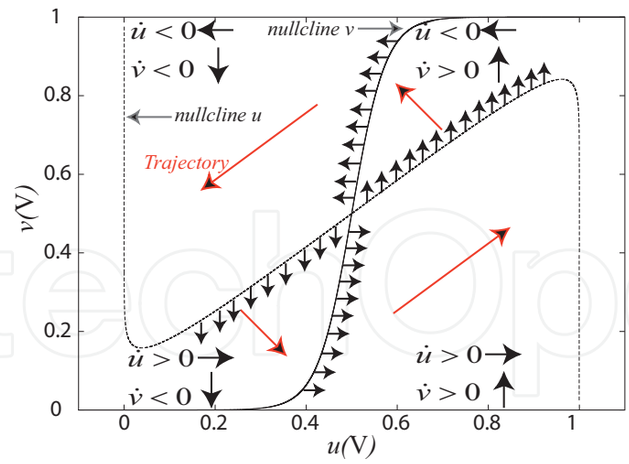

Fig. 2. u and v nullclines with vector field direction.

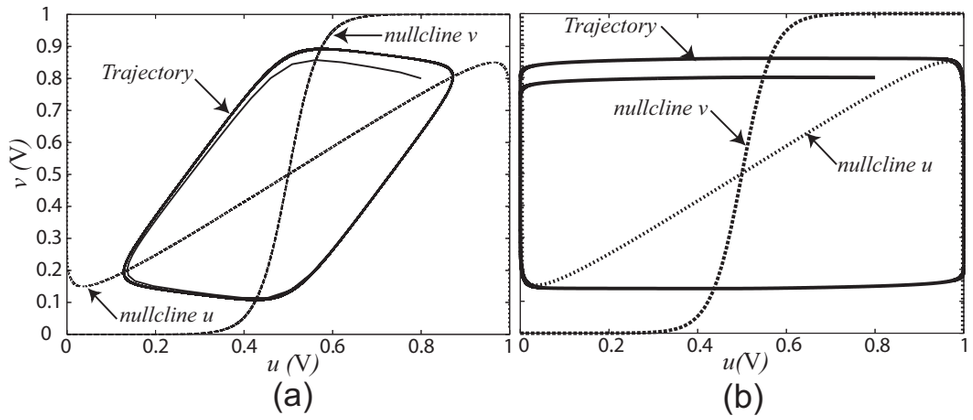

Fig. 3. Trajectory when a) $\tau = 1$ and b) $\tau << 1$.

Let us suppose that θ is set at a certain value where the critical temperature (T_c), which is proportional to A is 27°C. The critical temperature represents the threshold temperature we desire to measure. When θ changes, the v nullcline changes to a point where the system will be stable as long as the external temperature is higher than T_c. This is true because the system is unstable only when the fixed point exists in a negative resistive region of the u nullcline. The fixed point, defined by $\dot{u} = \dot{v} = 0$ is represented in the phase space by the intersection of the u nullcline with the v nullcline. At this point the trajectory stops because the vector field is zero, and the system is thus stable. On the other hand, when the external temperature is below T_c, the nullclines move, and this will correspond to a periodic solution to the system. In the phase space we can observe that the trajectory does not pass through the fixed point but describes a closed orbit or limit cycle, indicating that the system is oscillatory. Figure 4 shows examples when the system is stable (a) and oscillatory (b). In (a) the external temperature is greater than the critical temperature, hence, the trajectory stops when it reaches the fixed point, and the system is stable. In (b), where the temperature changes below the critical temperature, the trajectory avoids the fixed point, and the system becomes oscillatory.
Deriving the nullclines equation ($\dot{u} = 0$) and equaling to zero, I calculated the local minimum (u_-, v_-) and local maximum (u_+, v_+), representing the intersection point of the nullclines

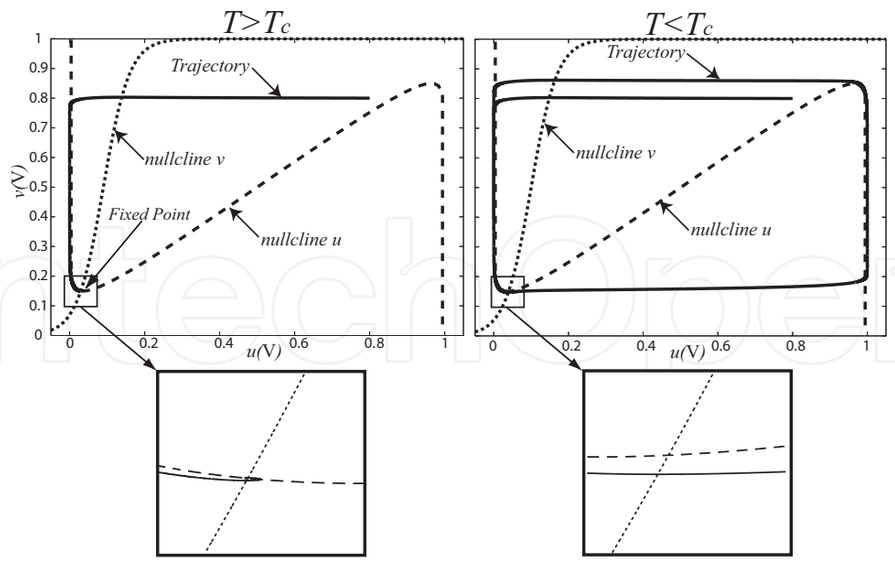

Fig. 4. Nullclines showing the fixed point and the trajectory when a) system is stable b) system is oscillatory.

given by:

$$u_{\pm} = \frac{1 \pm \sqrt{1-4A}}{2}, \tag{3}$$

$$v_{\pm} = u_{\pm} + A \ln\left(\frac{1}{u_{\pm}} - 1\right), \tag{4}$$

The nullclines giving the local minimum and local maximum $(u_{\pm}, v_{\pm})$ are shown in Fig. 5(a). From the local minimum and maximum equations (Eq. (3) and Eq. (4)), the nullcline equation ($\dot{v} = 0$) and remembering that A is proportional to temperature, I determined the relationship between θ and the temperature, to be given by:

$$\theta_{\pm} = u_{\pm} + A \ln\left(\frac{1}{v_{\pm}} - 1\right). \tag{5}$$

When $\tau << 1$ the trajectory jumps from one side to the other side of the u nullcline, so only along the u nullcline movement in the v direction are possible as shown in Fig. 3(b). It is necessary to emphasis this fact because this characteristic is necessary for the system operation; thus, I assume $\tau << 1$.

2.1 Stability of the Wilson-Cowan system

Wilson and Cowan (Wilson & Cowan, 1972) studied the properties of a nervous tissue modeled by populations of oscillating cells composed of two types of interacting neurons: excitatory and inhibitory ones. The Wilson-Cowan system has two types of temporal behaviors, i.e. steady state and limit cycle. According with the stability analysis in (Wilson & Cowan, 1972), the stability of the system can be controlled by the magnitude of the all the parameters. Equations (1) and (2) are a simplified set representing the Wilson-Cowan system

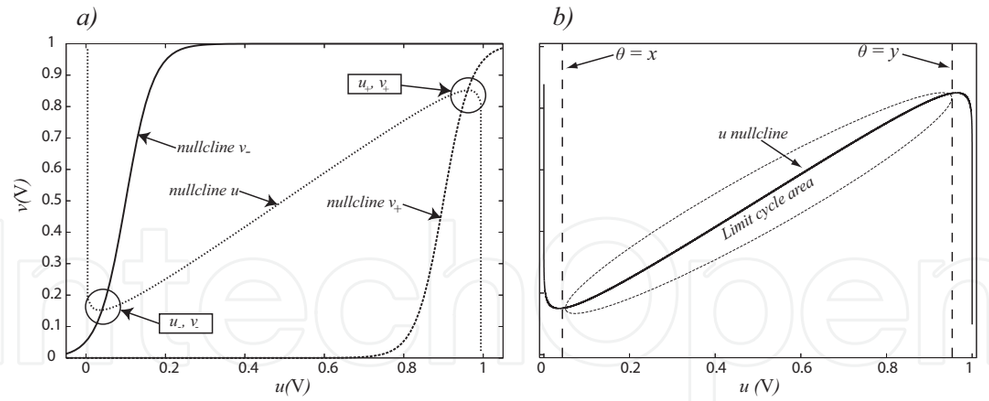

Fig. 5. a) u and v local maximum and local minimum. b) Threshold values x and y showing the area where the system is oscillatory.

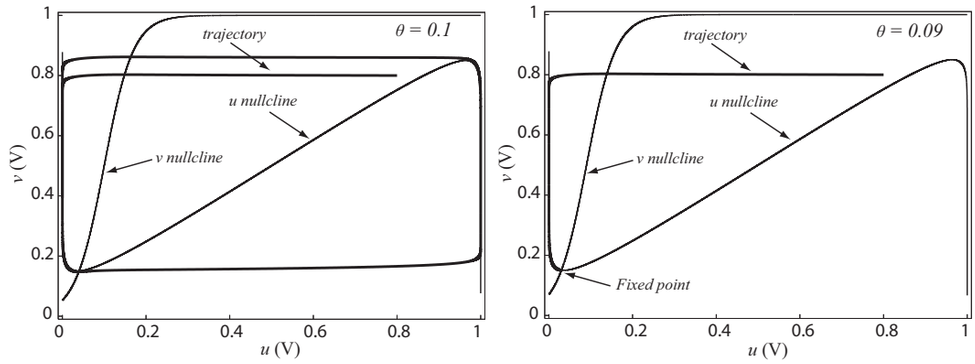

(a) (b)

Fig. 6. Nulclines and trajectories when a) $\theta = 0.1$ and b) $\theta = 0.09$.

equations with and excitatory node u and an inhibitory node v. The nullclines of this system, which are pictured in Fig. 2, are given by:

$$v = u + A \ln(\frac{1}{u} - 1) \tag{6}$$

for the u nullcline ((Eq. 1) = 0), and

$$v = \frac{e^{u/a}}{e^{u/a} + e^{\theta/A}} \tag{7}$$

for the v nullcline ((Eq. 2) = 0).
For an easy analysis, let us suppose that A is a constant. In this case, there are some important observations for the stability of the system.

- There is a low threshold value of θ bellow which the limit cycle activity can not occurs.
- There is a high threshold value of θ above which the system saturates and the limit cycle activity is extinguished.
- Between these two values (x for the lower threshold and y for the higher threshold), the system exhibit limit cycle oscillation.

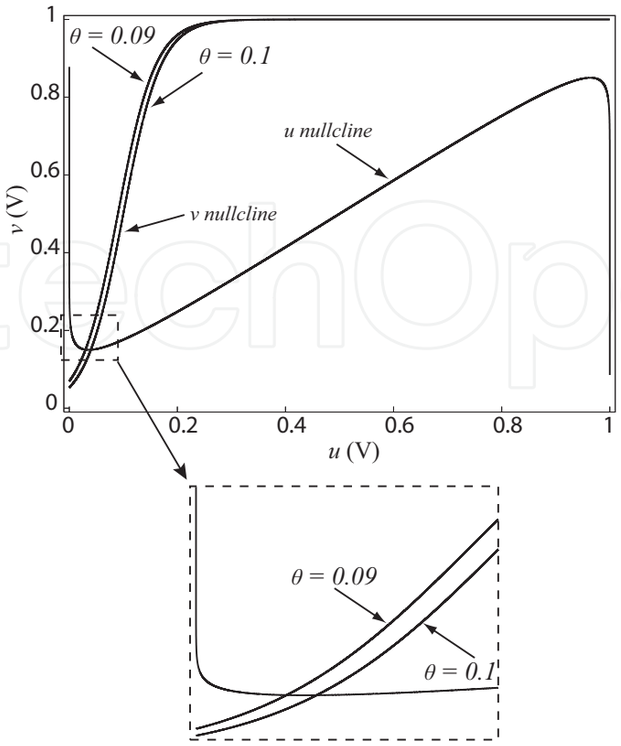

Fig. 7. v nullcline when $\theta = 0.1$ and $\theta = 0.09$.

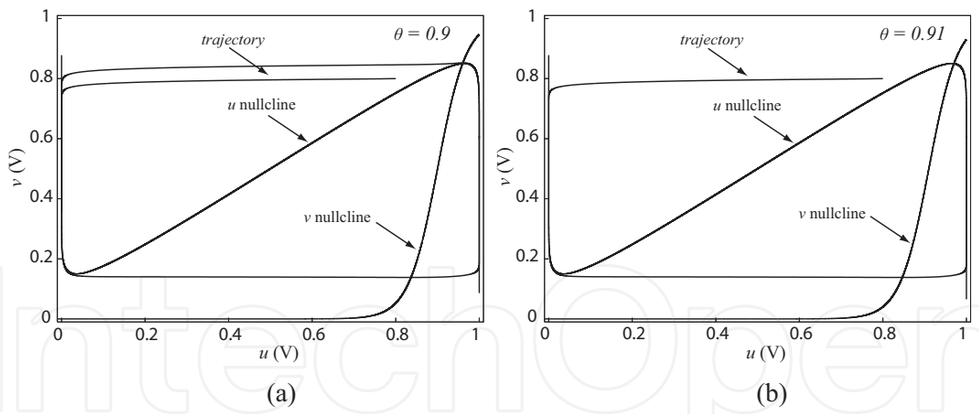

Fig. 8. Nulclines and trajectories when a) $\theta = 0.9$ and b) $\theta = 0.91$.

Let us suppose that the value of A is fixed to 0.03, in this cases, depending on the magnitude of the parameter θ (that is the external input of the system) the Wilson-Cowan oscillator will show different behaviors. Figure 5(b) shows the area inside which the system exhibits a limit cycle. The threshold values x and y are shown in the figure.
The nullclines and trajectories for different values of θ are shown in Figs. 6 and 8. In Figure 6 (a), θ was set to 0.1, we can observe that the system is exhibiting limit cycle oscillations. Thus, for this case the system is unstable. When the value of θ is reduce to 0.09, as show in Fig. 6 (b). It can be observed that the trajectory stops at the fixed point. The fixed point in this area is

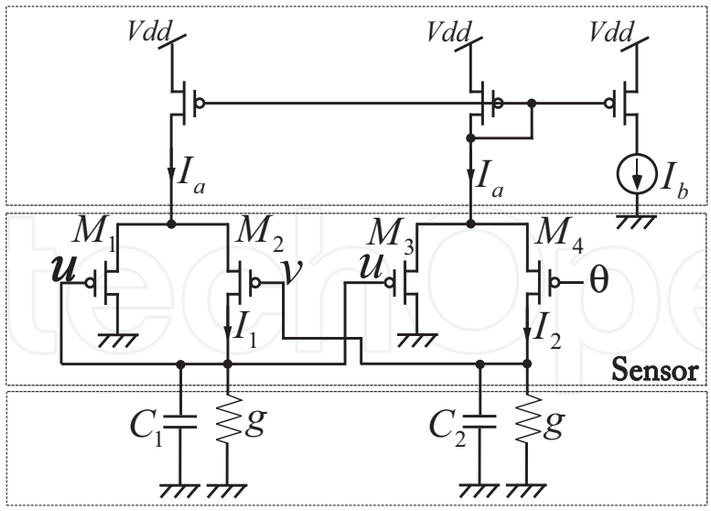

Fig. 9. Critical temperature sensor circuit.

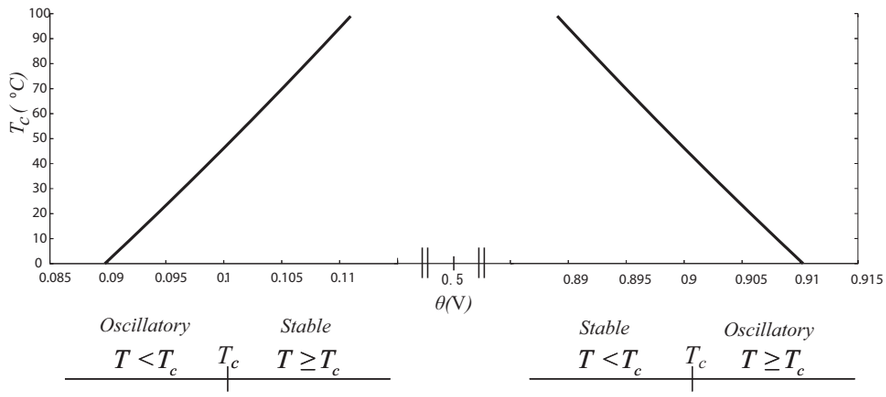

Fig. 10. Relation between $\theta_{\pm}$ and T_c.

an attractor, i.e. a stable fixed point. Thus, the system is stable. Figure 7 show the position of the v nullclines when $\theta = 0.09$ and $\theta = 0.1$. The other case (for a high threshold), is shown is Fig. 8. In figure 8 (a) θ is set to 0.9, at this point the system is oscillatory. When θ is increased, ($\theta = 0.91$) the system is stable.
We could observed that depending on the parameter θ (external input) the stability of the system can be controlled. It is important to note that the stability also depends on the magnitude of A, and that A is proportional to the temperature. These observations are the basis of the operation of the temperature sensor system.for example, by setting the value of the input θ, when the external temperature changes the system behavior also changes i.e. stable and oscillatory.

3. CMOS circuit

The critical temperature sensor circuit is shown in Fig. 9. The sensor section consists of two pMOS differential pairs ($M_1 - M_2$ and $M_3 - M_4$) operating in their sub-threshold region.

External components are required for the operation of the circuit. These components consist of two capacitors (C_1 and C_2) and two temperature-insensitive off-chip metal-film resistors (g). In addition, for the experimental purpose, two current mirrors were used as the bias current of differential pairs. Note that for the final implementation of our critical temperature sensor a current reference circuit with low-temperature dependence (Hirose et al., 2005) should be used.

Differential-pairs sub-threshold currents, I_1 and I_2, are given by (Liu et al., 2002):

$$I_1 = I_a \frac{\exp(\kappa u/v_T)}{\exp(\kappa u/v_T) + \exp(\kappa v/v_T)}, \tag{8}$$

$$I_2 = I_a \frac{\exp(\kappa u/v_T)}{\exp(\kappa u/v_T) + \exp(\kappa \theta/v_T)}, \tag{9}$$

where I_a represents the differential pairs bias current, v_T is the thermal voltage ($v_T = kT/q$), k is the Boltzmann's constant, T is the temperature, and q is the elementary charge.

The circuit dynamics can be determined by applying Kirchhoff's current law to both differential pairs, which is represented as follows:

$$C_1\dot{u} = -gu + \frac{I_a \exp(\kappa u/v_T)}{\exp(\kappa u/v_T) + \exp(\kappa v/v_T)}, \tag{10}$$

$$C_2\dot{v} = -gv + \frac{I_a \exp(\kappa u/v_T)}{\exp(\kappa u/v_T) + \exp(\kappa \theta/v_T)}, \tag{11}$$

where κ is the sub-threshold slope, C_1 and C_2 are the capacitances representing the time constants, and θ is bias voltage.

Note that Eqs. (10) and (11) correspond to the system dynamics (Eqs. (1) and (2)) previously explained. Therefore, applying the same analysis, I calculated the local minimum (u_-, v_-) and local maximum (u_+, v_+) for the circuit equations, expressed by:

$$u_\pm = \frac{I_a/g \pm \sqrt{(I_a/g)^2 - 4v_T I_a/(\kappa g)}}{2}, \tag{12}$$

$$v_\pm = u_\pm + \frac{v_T}{\kappa} \ln\left(\frac{I_a}{g u_\pm} - 1\right), \tag{13}$$

and the relationship between the external bias voltage (θ) and the external temperature (T):

$$\theta_\pm = u_\pm + \frac{v_T}{\kappa} \ln\left(\frac{I_a}{g v_\pm} - 1\right). \tag{14}$$

where the relation with the temperature is given by the thermal voltage defined by $v_T = kT/q$. At this point the system temperature is equal to the critical temperature which can be obtained from:

$$T_c = \frac{q\kappa(\theta_\pm - u_\pm)}{k \ln\left(\frac{I_a}{g v_\pm} - 1\right)}. \tag{15}$$

The threshold temperature T_c can be set to a desired value by adjusting the external bias voltage (θ). The circuit changes its dynamic behavior, i.e., oscillatory or stationary behaviors, depending on its operation temperature and bias voltage conditions. At temperatures lower than T_c the circuit oscillates, but the circuit is stable (does not oscillate) at temperatures higher than T_c. Figure 10 shows the relation between the bias voltage $\theta_\pm$ and the critical temperature

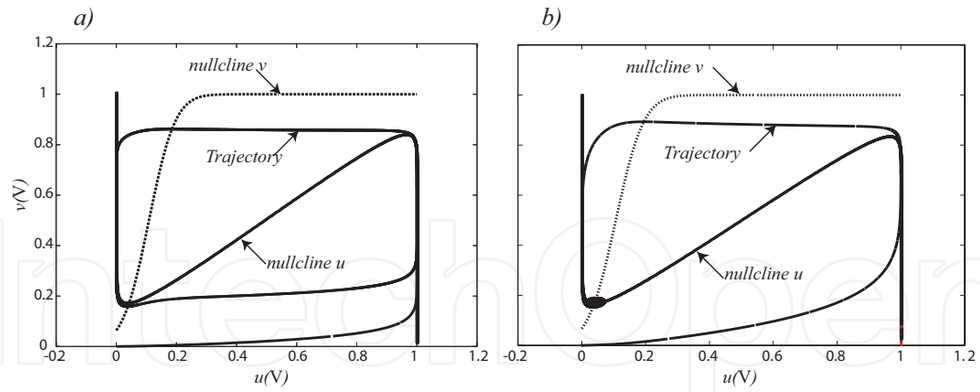

Fig. 11. Trajectory and nullclines obtained through simulation results when a) the system is oscillatory. b) the system is stationary

T_c with $\kappa = 0.75$; θ_- for u and v local minimums and θ_+ for u and v local maximums. When θ_- is used to set T_c, the system is stable at external temperatures higher than T_c; while when θ_+ is used, the system is stable when the external temperature is lower than T_c and oscillatory when it is higher than T_c.

4. Simulations and experimental results

Circuit simulations were conducted by setting C_1 and C_2 to 0.1 pF and 10 pF, respectively, g to 1 nS, and reference current (I_b) to 1 nA. Note that for the numerical and circuit simulations, two current sources were used instead of the current mirrors. The parameter sets I used for the transistors were obtained from MOSIS AMIS 1.5-μm CMOS process. Transistor sizes were fixed at $L = 40$ μm and $W = 16$ μm. The supply voltage was set at 5 V. Figure 11(a) shows the nullclines and trajectory of the circuit with the bias voltage (θ) set at 200 mV and the external temperature (T) set at 27°C; the system was in oscillatory state. Figure. 11(b) shows the nullclines when the system is stationary with the bias voltage (θ) set at 90 mV.
The output waveform of u for different temperatures is shown in Fig. 12. The bias voltage θ was set to 120 mV, when the external temperature was 20°C the circuit was oscillating, but when the temperature increases up to 40°C the circuit becomes stable. Figure 13 shows the simulated oscillation frequencies of the circuit as a function of the temperature, the bias voltage set to 120 mV. The frequency was zero when the temperature was above the critical temperature $T_c = 36$°C, and for temperatures lower than T_c the frequency increased, as shown in the figure.
Through circuit simulations, by setting the values for the critical temperature (T_c) and changing the bias voltage (θ) until the system changed its state, I established a numerical relation between T_c and θ. When comparing this relationship between θ and T_c obtained through different methods, I found a mismatch between the numerical simulations and the circuit simulations. This difference might be due to the parameters that are included in the SPICE simulation but omitted in the numerical simulation and theoretical analysis. Many of these parameters might be temperature dependent; thus, their value changes with temperature, and as a result of this change, the T_c characteristic changes. The difference between the two simulations is shown in Fig. 14

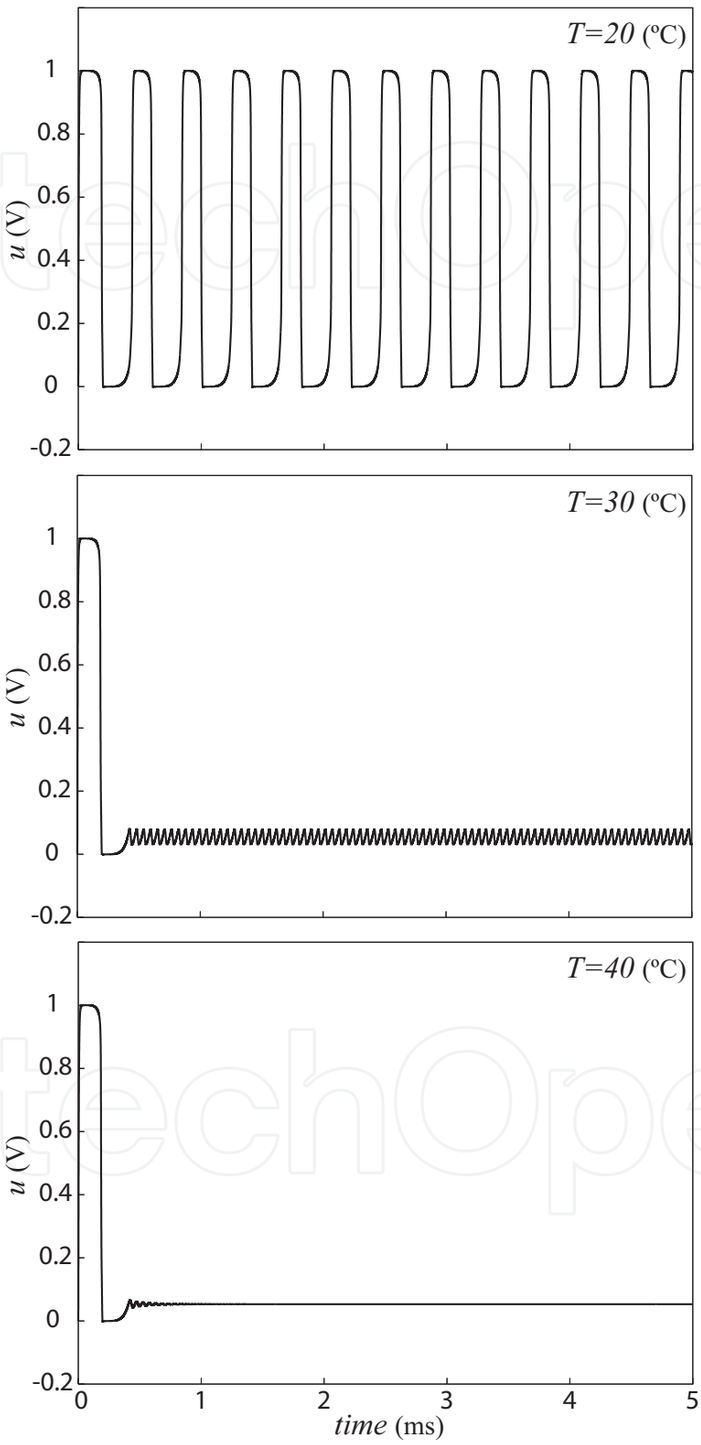

Fig. 12. Waveform of u at different temperatures (from $T = 20°C$ to $T = 40°C$).

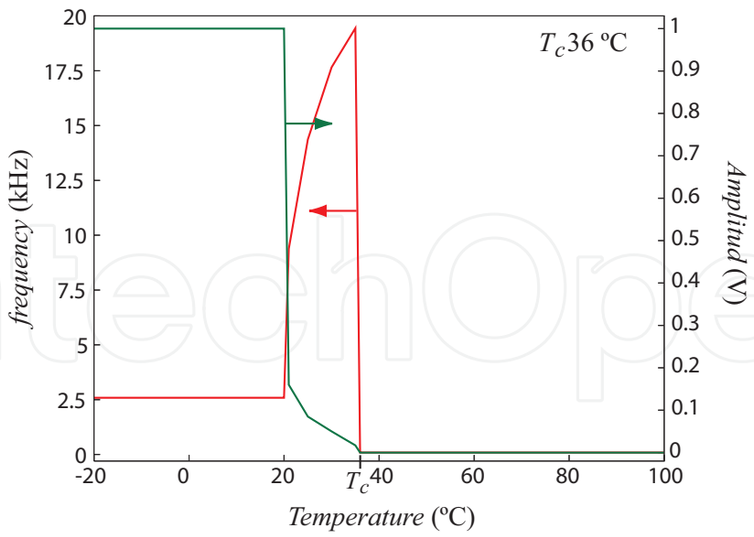

Fig. 13. Oscillation frequencies of the circuit. ($T_c = 36°$C).

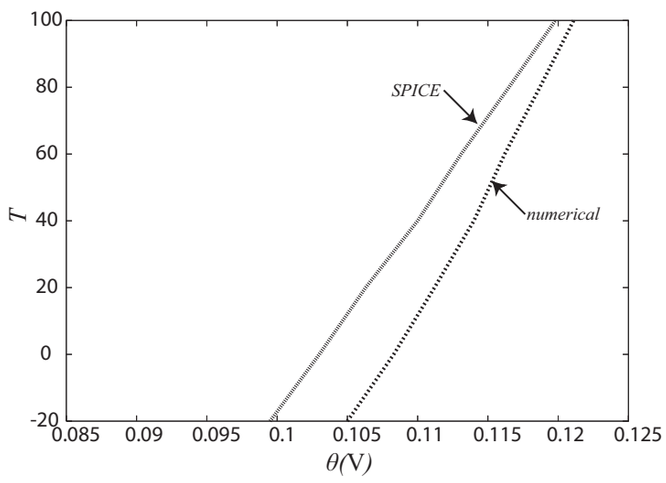

Fig. 14. Relation between $\theta_{\pm}$ and T_c obtained through numerical and circuit simulations.

I successfully demonstrated the critical temperature sensor's operation using discrete MOS circuits. Parasitic capacitances and a capacitance of 0.033 μF were used for C_1 and C_2 respectively, and the resistances (g) were set to 10 MΩ. The input current (I_b) for the current mirrors was set to 100 nA and I obtained an output current (I_a) of 78 nA.
Measurements were performed at room temperature (T = 23°C). With the bias voltage (θ) set to 500 mV the voltages of u and v were measured. Under these conditions, the circuit was oscillating. The voltages of u and v for different values of θ were also measured. The results showed that for values of θ lower than 170 mV, the circuit did not oscillate (was stable), but that for values higher than 170 mV, the circuit became oscillatory. Figures 15 and 16 shows the oscillatory and stable states of u and v with θ set to 170 and 150 mV, respectively.
In addition, I also measured the nullclines (steady state voltage of the differential pairs). The v nullcline (steady state voltage v of differential pair $M_3 - M_4$) was measured by applying a variable DC voltage (from 0 to 1 V) on u and measuring the voltage on v. For the measurement

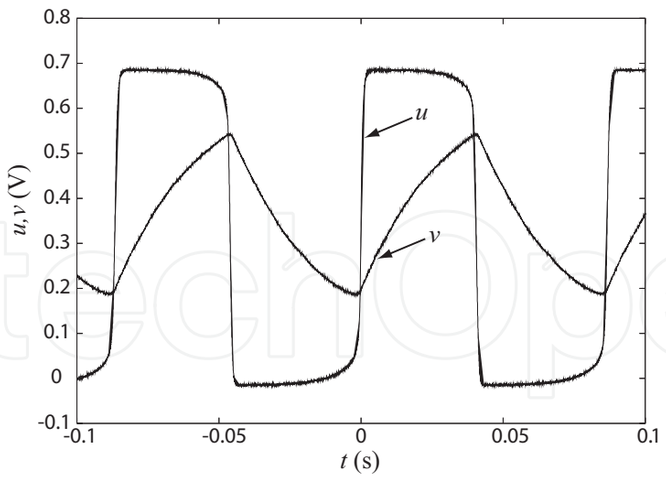

Fig. 15. Experimental results: θ =170 mV at T= 23°C (oscillatory state).

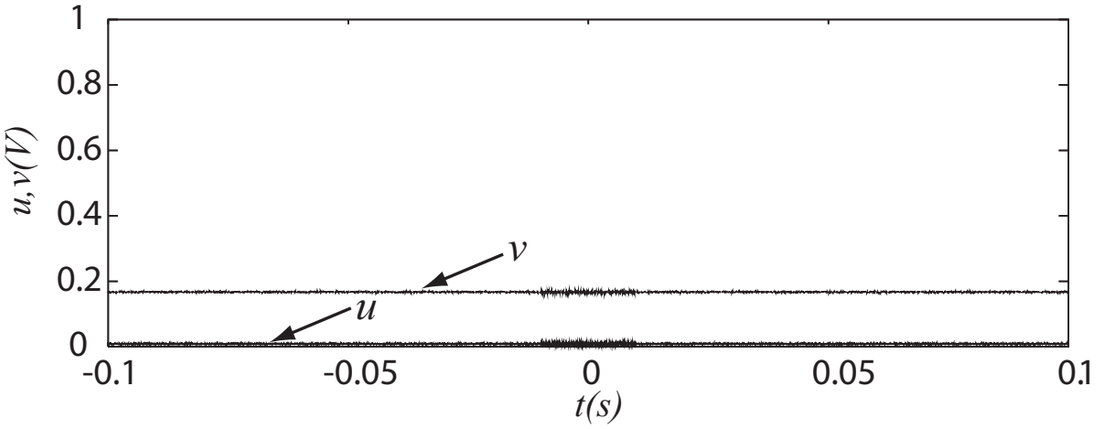

Fig. 16. Experimental results: θ =150 mV at T= 23°C (stationary state).

of the u nullcline (steady state voltage u of differential pair $M_1 - M_2$), a special configuration of the first differential pair of the circuit was used. Figure 17 shows the circuit used for the u nullcline measurement. I applied a variable DC voltage (from 0 to 1 V) on v. For each value of v I changed the voltage on u_1 (from 0 to 1) and then measured the voltage on u_o and u_1. This enabled us to obtain the u nullcline by plotting the points where u_o and u_1 had almost the same value. In this way, I obtained a series of points showing the shape of the u nullcline. The series of points was divided into three sections, and the average was calculated to show the u nullcline. Figure 18 shows the u nullcline divided into the three sections used for the average calculation. The trajectory and nullclines of the circuit with θ set to 500 mV are shown in Fig. 19.

Notice that in the experimental results there is a difference in the amplitude of the potentials u and v with respect to results obtained from the numerical and circuit simulations. This is due to the difference in the bias current of the differential pairs. From Eqs. (12) and (13), we can see that by making g and I_b (used in numerical and circuit simulations) the same value, they cancel each other out; however, the output currents of the current mirrors were in the

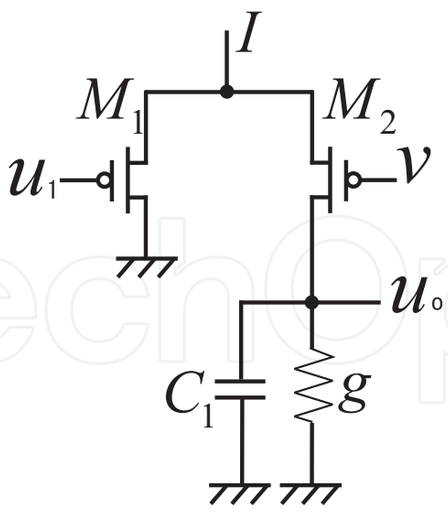

Fig. 17. Circuit used for calculation of the u nullcline.

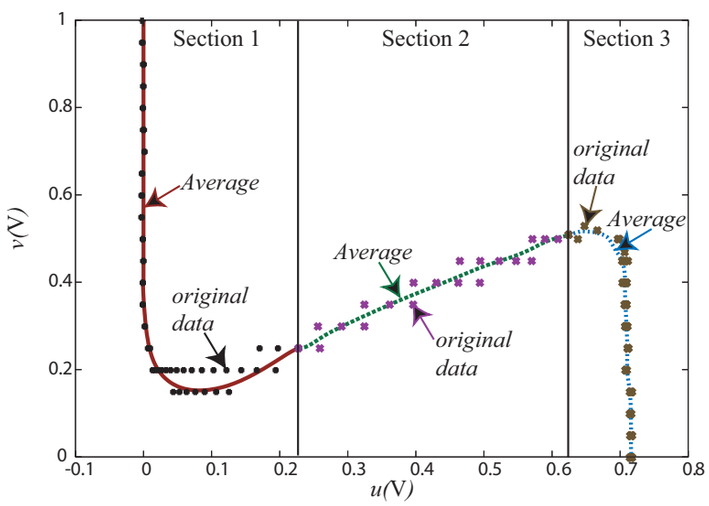

Fig. 18. Sections used for the calculation of the u nullcline.

order of 78 nA, and g was set to 100 nS. This difference caused the decrease in the potentials amplitudes, as shown in Figs.11 and 19.

Measurements performed at different temperatures were made. The bias voltage (θ) was set to a fixed value and the external temperature was changed to find the value of the critical temperature (T_c) where the circuit changes from one state to the other. With the bias voltage θ set to 170 mV at room temperature (T = 23°C), the circuit oscillated. When the external temperature was increased to (T = 26°C), the circuit changed its state to stationary (did not oscillate). Once again, when the external temperature was decreased one degree (T = 25°C), the circuit started to oscillate; therefore, the critical temperature was T_c = 26°C. Measures of the critical temperature (T_c) for different values of the bias voltage (θ) were made.

In order to compare experimental results with, SPICE results and theoretical ones, the actual κ (subthreshold slope) of the HSPICE model was measured and found to be in the order of 0.61. The critical temperature for each value of θ obtained experimentally compared with the critical

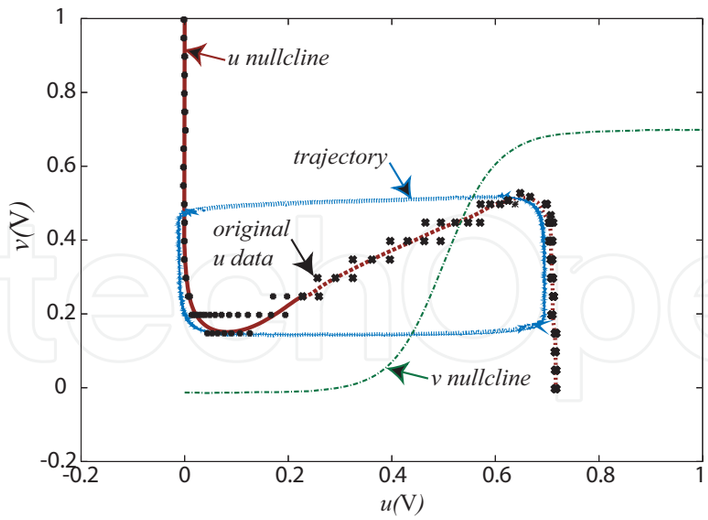

Fig. 19. Experimental nullclines and trajectory.

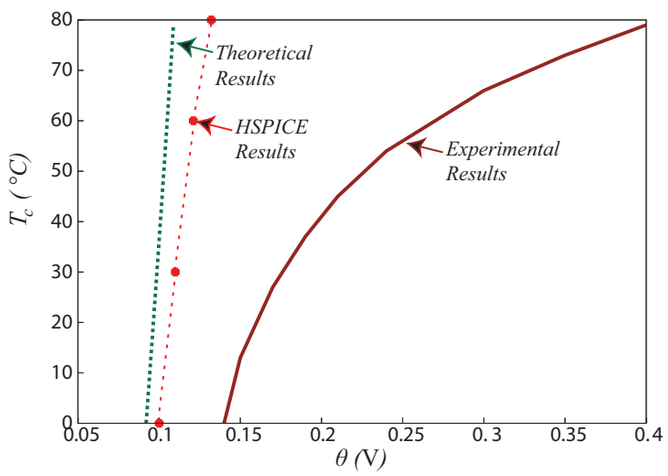

Fig. 20. Bias voltage vs temperature, experimental results.

temperature obtained with theoretical analysis using Eq. (14) (with $\kappa = 0.61$) is shown in Fig. 20. The curves have positive slopes in both cases. This is because the temperature difference between one value of bias voltage and the other decreases as the bias voltage increases. For θ= 140 and 150 mV the experimentally obtained critical temperatures (T_c) are 0°C and 13°C, respectively, a difference of 13°C. For θ= 240 and 250 mV the critical temperatures (T_c) are 54°C and 56°C, respectively: a difference of only 2°C.

The difference between the experimental, HSPICE, theoretical results is due to the leak current caused by parasitic diodes between the source (drain) and the well or substrate of the discrete MOS devices, and the mismatch between the MOS devices. In addition, because of the leak current, when temperature increases, the stable voltages of u and v also increase. Figures 21(a) and 21(b) shows the stationary state with θ set to 140 mV and temperature set to 23 and 75°C, respectively.

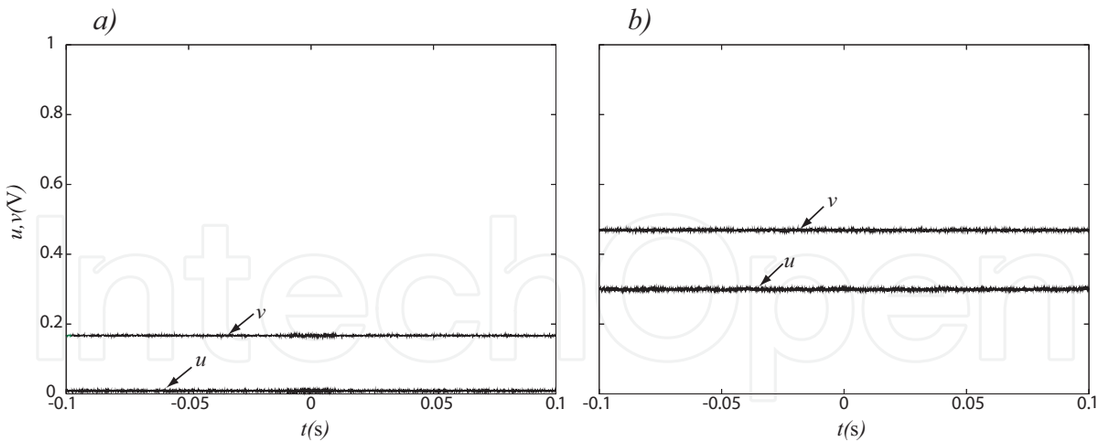

Fig. 21. Stationary state with a) θ= 140 mV and T= 23°C. b) θ= 140 mV and T= 75°C

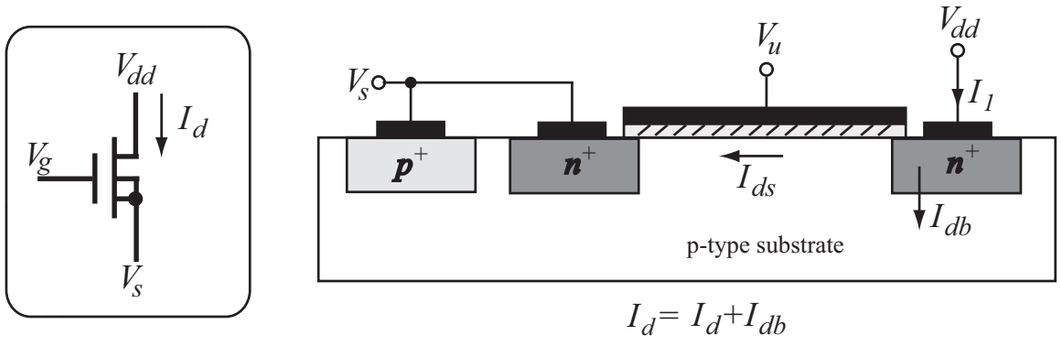

Fig. 22. nMOS transistor structure showing leak current

5. nMOS Transistor with temperature dependence

The structure of a nMOS transistor showing the temperature-sensitive drain to bulk leakage current (I_{db}) is shown in Fig. 22. The drain current of the transistor is thus given by the sum of the drain-bulk current (I_{db}) and the channel current (I_{ds}).

$$I_d = I_{ds} + I_{db} \tag{16}$$

and remembering that the saturated drain to source current when the transistor is operating in the subthreshold region is given by

$$I_{ds} = I_0 e^{\kappa(V_g - V_s)/V_T} \tag{17}$$

the drain current becomes

$$I_d = I_0 e^{\kappa(V_g - V_s)/V_T} + I_{db} \tag{18}$$

where I_0 represents the fabrication parameter, and V_s the common source nd bulk voltage. The drain-bulk current (I_{db}) is given by:

$$I_{db} = G_{db}(V_{dd} - V_b) \tag{19}$$

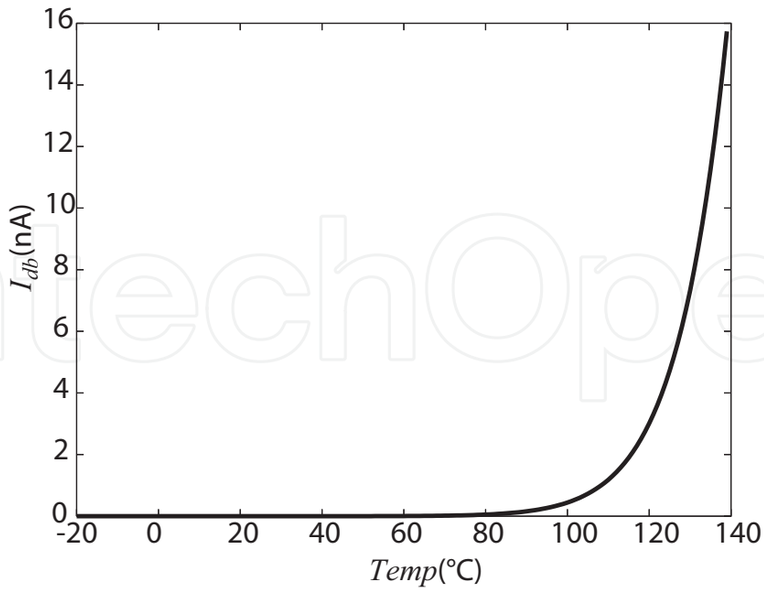

Fig. 23. Drain-bulk current I_{db} vs *Temperature*.

where V_{dd} is the supply voltage, V_b the bulk potential, and G_{db} the temperature-dependent drain-bulk conductance expressed as:

$$G_{db} = G_S e^{\frac{E_g(T_{nom})}{V_{T_{nom}}} - \frac{E_g(T)}{V_T}} \tag{20}$$

where G_S represents the bulk junction saturation conductance (1×10^{-14}), $E_g(X)$ is the energy gap, and T_{nom} the nominal temperature (300.15 K). The temperature dependence of the energy gap is modeled by

$$E_g(T) = E_g(0) - \frac{\alpha T^2}{\beta + T} \tag{21}$$

Si experimental results give $E_g(0) = 1.16$ eV, $\alpha = 7.02 \times 10^{-4}$, and $\beta = 1108$.
Numerical simulations where carried out. Figure 23 shows the drain-bulk current of a single transistor as the temperature changes. We can observe that when the temperature is less than 80 $^\circ C$ the drain-bulk (I_{db}) current is in the order of pF ($\approx$ 30 pF), but as temperature increases, I_{db} also increases in an exponential manner reaching values in the order of nA ($\approx$ 16 nA for $T = 140\ ^\circ C$).
The same analysis can be applied to pMOS transistors, but in addition the leak current from the p-substrate to the n-Well is added to the drain current.

6. Differential pair with temperature dependence

Figure 24 shows a differential pair circuit consisting of two nMOS transistors (m_1 and m_2), and an ideal current source (I_b). According with the analysis done in the previous section, the drain currents (I_1 and I_2) are

$$I_1 = I_0 e^{\kappa(u - V_s)/V_T} + I_{db} \tag{22}$$

$$I_2 = I_0 e^{\kappa(v - V_s)/V_T} + I_{db} \tag{23}$$

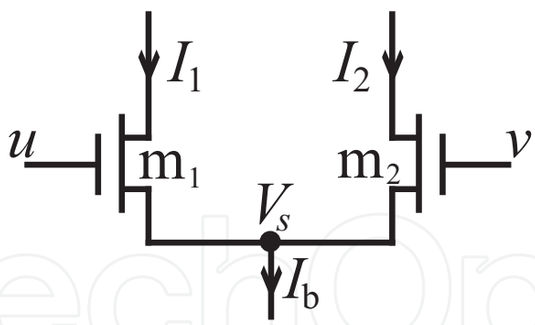

Fig. 24. Differential pair.

Since $I_b = I_1 + I_2$, we obtain

$$e^{-\kappa V_s/V_T} = \frac{I_b - 2I_{db}}{I_0(e^{\kappa u/V_T} + e^{\kappa v/V_T})} \tag{24}$$

From Eqs. (22) and (23), the drain currents become

$$I_1 = \frac{(I_b - 2I_{db})e^{\kappa u/V_T}}{e^{\kappa u/V_T} + e^{\kappa v/V_T}} + I_{db} \tag{25}$$

$$I_2 = \frac{(I_b - 2I_{db})e^{\kappa v/V_T}}{e^{\kappa u/V_T} + e^{\kappa v/V_T}} + I_{db} \tag{26}$$

From Eq. (24) the common source voltage V_s is

$$V_s = \frac{V_T}{\kappa}\left\{\ln I_0 + \ln\left(e^{\kappa u/V_T} + e^{\kappa v/V_T}\right) - \ln\left(I_b - 2I_{db}\right)\right\} \tag{27}$$

Equations (25) and (26) were plotted and compared with the SPICE simulations results (see figure 25). I used the MOSIS AMIS 1.5-μm CMOS parameters (LEVEL 3). Transistor sizes were set to $W/L = 4\ \mu$m$/1.6\ \mu$m. I_b was set to 100 nA, and v was set to 0.5 V. From the SPICE simulations, the measured κ 0.47, I_0 was 18.8 pA when $T = 300.15\ ^\circ K$, and 62.6 pA when $T = 350.15\ ^\circ K$. We can observe that the theoretical results agreed with the SPICE results.

7. Dynamics of the CTS circuit

The critical temperature sensor circuit is shown in Fig. 9. The circuit dynamics Eqs. (10) and (11) with the temperature dependence analysis become

$$C_1\dot{u} = -gu + \frac{(I_a - 2I_{db} - 2I_{ws})\exp(\kappa u/v_T)}{\exp(\kappa u/v_T) + \exp(\kappa v/v_T)} + I_{db} + I_{ws}, \tag{28}$$

$$C_2\dot{v} = -gv + \frac{(I_a - 2I_{db} - 2I_{ws})\exp(\kappa u/v_T)}{\exp(\kappa u/v_T) + \exp(\kappa \theta/v_T)} + I_{db} + I_{ws}, \tag{29}$$

To confirm the effect of the leak currents in the temperature sensor system, I conducted a comparative analysis between HSPICE and the theoretical results without and with leak current. The comparison between HSPICE results and theoretical results without leak currents effect with the bias voltage θ set to 0.5 V and the external temperature set to $T = 127\ ^\circ C$, is shown in Fig. 26(a). It can be seen that in this case the results between the theory and the SPICE are very different, but in the same conditions when the effect of the leak current is include in the theory the results are very similar, Fig. 26(b).

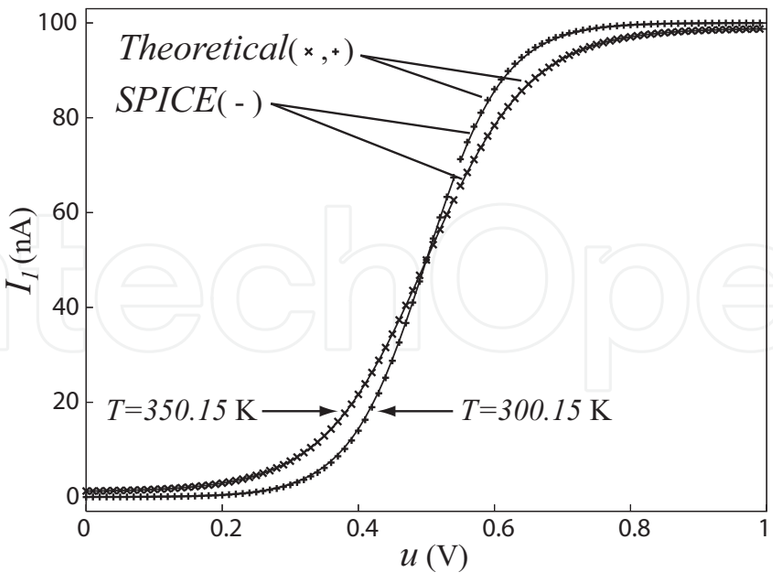

Fig. 25. Theoretical and SPICE results of differential pair's current I_1 when temperature is 300.15 K and 400.15 K.

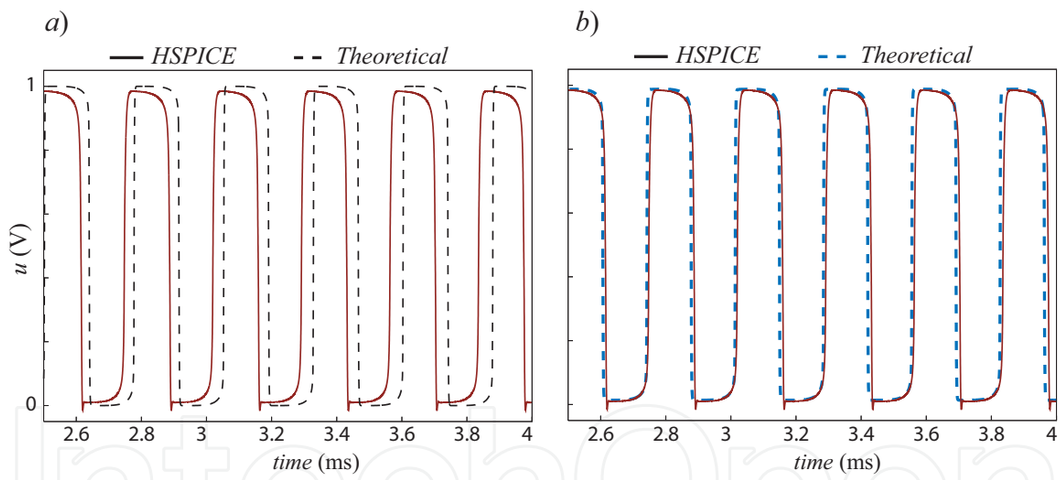

Fig. 26. Comparison of CTS oscillations, between HSPICE results and theoretical results with $T = 127\ ^{\circ}$C. a) without leak currents. b) with leak currents.

8. Conclusion

This research focused on the studied and the implementation of artificial neural systems. As a small contribution, to reach the final goal all researchers have in common, *the building of an artificial brain*. To accomplish this, I proposed the design of a critical temperature sensor strongly inspired by the operation of biological neurons of sea slugs and snails.
The sensor consists of a sub-threshold CMOS circuit that changes its dynamic behavior, i.e., oscillatory or stationary behaviors, at a given threshold temperature.

I analyzed the circuit's operation theoretically, giving a mathematical model of its operation. Also, I conducted extensive numerical and circuit simulations. Furthermore, I demonstrated the operation of the circuit, using discrete MOS devices through experimental results.
The threshold temperature, can be set to a desired value by adjusting the external bias voltage (θ). I demonstrated that the circuit changed its state between oscillatory and stationary when the external temperature was lower or higher than the threshold temperature. Moreover, I experimentally calculated the circuit nullclines, indicating the trajectory of the circuit when it is in oscillatory state.

Future work

This kind of system can be used as a sensory system for first stage of perception (a receptor). In other words a temperature receptor circuit, which detects a tranduces physical stimuli (temperature) into electrical impulses.
The combination of such kind of simple circuit will allow the design of hardware system that are capable of detecting, transforming, transferring, processing and interpreting sensory stimuli. The possibility to built complex neuromorphic systems which sense and interact with the environment will hopefully contribute to advancements in both, basic research and commercial applications. This technology is likely to become instrumental for research on computational neuroscience, and for practical applications that involve sensory signal processing, in uncontrolled environments

9. References

Asai, T., Kanazawa, Y., & Amemiya, Y. (2003). A subthreshold MOS neuron circuit based on the Volterra system. *IEEE Trans. Neural Networks*, Vol. 14(5): 1308-1312.

Barranco, B. L., Sinencio, E. S., Vazquez, A. R., & Huertas, J. L. (1991) A CMOS implementation of FitzHugh-Nagumo neuron model. *IEEE J. Solid-State Circuits.*, Vol. 26: 956-965.

Douglas, R., Mahowald, M., & Mead, C., (1995). Neuromorphic analogue VLSI. *Ann. Rev. Neurosci.* Vol. 18: 255-281.

Fletcher D. S. & Ram L. J. (1990). High temperature induces reversible silence in Aplysia R15 bursting pacemaker neuron. *Comp. Biochem. Physiol.*. Vol. 98A: 399-405.

Gopel, W., Hesse, J., & Zermel J. N. (1990). Sensors. A comprehensive survey, *Thermal sensors* T. Ricolfi and J. Scholz, Eds. Vol. 4, VCH, pp. .

Hirose, T., Matsuoka, T., Taniguchi, K., Asai, T., & Amemiya, Y. (2005). Ultralow-power current reference circuit with low-temperature dependence. *IEICE Transactions on Electronics*, Vol. E88-C(6): 1142-1147.

Meador J. L. & Cole, C. S. (1989). A low-power CMOS circuit which emulates temporal electrical properties of neurons. *Advances in Neural Information Processing Systems 1.*, D. S. Touretzky, Ed., Los Altos, CA: Morgan Kaufmann, pp.678-685.

Murray, A. F., Hamilton, A., & Tarassenko, L. (1989). Programmable analog pulse-firing neural networks. *Advances in Neural Information Processing Systems 1.*, D. S. Touretzky, Ed., Los Altos, CA: Morgan Kaufmann, pp. 671-677. .

Liu, S., Kramer, J., Indiveri, G., Delbruck, T., & Douglas, R. (2002). Analog VLSI: circuit and principles. *Massachusetts Institute of Technology Cambridge*, Massachusetts. The MIT press, London, England.

Ryckebusch, S., Bower, J. M., & Mead, C. (1989). Modeling small oscillating biological networks in analog VLSI, In *Advances in Neural Information Processing Systems 1.*, D. S. Touretzky, Ed., Los Altos CA: Morgan Kaufmann, pp. 384-393.

Wang, C. C., Akbar, S. A., & Madou M. J. (1998). Ceramic based resistive sensors. *Journal of Electroceramics*, Vol. 2(4): 273-282.

Wilson, H. R. & Cowan, J. D. (1972). Excitatory and inhibitory interactions in localized populations of model neurons. *Biophys. J.*, Vol. 12: 1-24

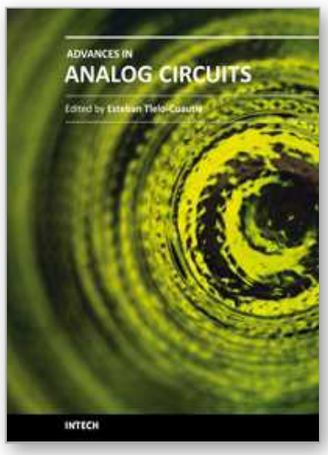

Advances in Analog Circuits

Edited by Prof. Esteban Tlelo-Cuautle

ISBN 978-953-307-323-1
Hard cover, 368 pages
Publisher InTech
Published online 02, February, 2011
Published in print edition February, 2011

This book highlights key design issues and challenges to guarantee the development of successful applications of analog circuits. Researchers around the world share acquired experience and insights to develop advances in analog circuit design, modeling and simulation. The key contributions of the sixteen chapters focus on recent advances in analog circuits to accomplish academic or industrial target specifications.

How to reference

In order to correctly reference this scholarly work, feel free to copy and paste the following:

Gessyca M., Tovar Nunez (2011). Analog Circuits Implementing a Critical Temperature Sensor Based on Excitable Neuron Models, Advances in Analog Circuits, Prof. Esteban Tlelo-Cuautle (Ed.), ISBN: 978-953-307-323-1, InTech, Available from: http://www.intechopen.com/books/advances-in-analog-circuits/analog-circuits-implementing-a-critical-temperature-sensor-based-on-excitable-neuron-models

INTECH
open science | open minds

InTech Europe
University Campus STeP Ri
Slavka Krautzeka 83/A
51000 Rijeka, Croatia
Phone: +385 (51) 770 447
Fax: +385 (51) 686 166
www.intechopen.com

InTech China
Unit 405, Office Block, Hotel Equatorial Shanghai
No.65, Yan An Road (West), Shanghai, 200040, China
中国上海市延安西路65号上海国际贵都大饭店办公楼405单元
Phone: +86-21-62489820
Fax: +86-21-62489821

IntechOpen